———, "Mixing in Turbulent Fields," in *Turbulence in Mixing Operations*, R. S. Brodkey, ed., Chapt. II, Academic Press, New York (1975).
———, M. F. Cohen, Capt. J. S. Knox, G. L. McKee, K. N. MeKelvey, M. A. Rao, S. Zakanycz, and H.-n. Yieh, "Turbulence Measurements in Shear Flow Liquid Systems," Proc. Symp. Turbulence Measurements in Liquids, Dept. Ch. E., Univ. of Missouri-Rolla (1971).
Corrsin, S., "The Isotropic Turbulent Mixer: Part II. Arbitrary Schmidt Number," *AIChE J.*, **10**, 870 (1964).
Gegner, J. P., and R. S. Brodkey, "Dye Injection at the Centerline of a Pipe," *ibid.*, **12**, 817 (1966).
Gibson, C. H., and W. H. Schwarz, "Detection of Conductivity Fluctuations in a Turbulent Flow Field," *J. Fluid Mech.*, **16**, 357 (1963); "The Universal Equilibrium Spectra of Turbulent Velocity and Scalar Fields," *ibid.*, 365.
Grant, H. L., B. A. Hugehes, W. M. Vogel, and A. Moilliet, "The Spectrum of Temperature Fluctuations in Turbulent Flow," *ibid.*, **34**, 423 (1968).
Harris, I. J., and R. D. Srivastava, "The Simulation of Single Phase Tubular Reactors with Incomplete Reactant Mixing," *Can. J. Chem. Eng.*, **46**, 66 (1968).
Hinze, J. O., "Turbulence," pp. 237-8, McGraw-Hill, New York (1969).
Kattan, A., and R. J. Adler, "A Stochastic Mixing Model for Homogeneous, Turbulent, Tubular Reactors," *AIChE J.*, **13**, 580 (1967).
Keeler, R. N., L. E. Petersen, and J. M. Prausnitz, "Mixing and Chemical Reaction in Turbulent Flow Reactors," *ibid.*, **11**, 221 (1965).
Lee, J., "Turbulent Motion and Mixing," Ph.D. dissertation, The Ohio State Univ., Columbus (1962).
———, and R. S. Brodkey, "Light Probe for the Measurement of Turbulent Concentration Fluctuations," *Rev. Sci. Instr.*, **34**, 1086 (1963).
———, "Turbulent Motion and Mixing in a Pipe," *AIChE J.*, **10**, 187 (1964).
Mao, K. W. and H. L. Toor "A Diffusion Model for Reactions with Turbulent Mixing," *ibid.*, **16**, 49 (1970).
———, "Second-Order Chemical Reactions with Turbulent Mixing," *Ind. Eng. Chem. Fundamentals*, **10**, 192 (1971).
McKelvey, K. N., "Turbulent Mixing with Chemical Reaction," Ph.D. dissertation, The Ohio State Univ., Columbus (1968).
Nye, J. O., and R. S. Brodkey, "The Scalar Spectrum in the Viscous-Convective Subrange," *J. Fluid Mech.*, **29**, 151 (1967a).
———, "Light Probe for Measurement of Turbulent Concentration Fluctuations," *Rev. Sci. Instr.*, **38**, 26 (1967b).
O'Brien, E. E., "Postulate of Statistical Independence for Decaying Reactants in Homogeneous Turbulence," *Phys. Fluids*, **12**, 1999 (1969).
Patterson, G. K., "Simulating Turbulent-field Mixers and Reactors, in *Turbulence in Mixing Operations*," Chapt. V, R. S. Brodkey, ed., Academic Press, New York (1975).
Rao, D. P., and I. J. Dunn, "A Monte Carlo Coalescence Model for Reaction with Dispersion in a Tubular Reactor," *Chem. Eng. Sci.*, **25**, 1275 (1970).
Rao, D. P., and L. L. Edwards, "On the Diffusion Model of Mao and Toor," *AIChE J.*, **17**, 1264 (1971).
Toor, H. L., "Mass Transfer in Dilute Turbulent and non-Turbulent Systems with Rapid Irreversible Reactions and Equal Diffusivities," *ibid.*, **8**, 70 (1962).
———, "Turbulent Mixing of Two Species With and Without Chemical Reactions," *Ind. Eng. Chem. Fundamentals*, **8**, 655 (1969).
———, "The Non-Premixed Reaction; A + B Products," in *Turbulence in Mixing Operations*, Chapt. III, R. S. Brodkey, ed., Academic Press, New York (1975).
Torrest, R. S., and W. E. Ranz, "Improved Conductivity System for Measurement of Turbulent Concentration Fluctuations," *Ind. Eng. Chem. Fundamentals*, **8**, 810 (1969).
———, "Concentration Fluctuations and Chemical Conversion Associated with Mixing in Some Turbulent Flows," *AIChE J.*, **16**, 930 (1970).
Vassilatos, G., and H. L. Toor, "Second-Order Chemical Reactions in a Nonhomogeneous Turbulent Field," *ibid.*, **11**, 666 (1965).
Zakanycz, S., "Turbulence and the Mixing of Binary Gases," Ph.D. dissertation, The Ohio State Univ., Columbus (1971).
Yieh, H.-n., "Turbulent Mixing with Chemical Reaction," Ph.D. dissertation, The Ohio State Univ., Columbus (1970).

Manuscript received April 30, 1975; revision received August 13, and accepted August 14, 1975.

Electroosmosis and Electrolyte Conductance in Charged Microcapillaries

Interactions between the electrostatic double layer and transport rates in long capillary pores were investigated experimentally. Track-etched mica sheets with extremely narrow pore size distribution and large length-to-radius ratio were used as model membranes to examine the electrokinetic phenomena enhanced conduction and electroosmosis as a function of pore size and electrolyte (potassium chloride) concentration. Of experimental significance was that the capillary pores were of radius comparable to or even less than the solution Debye length parameter even at moderate (10^{-4} — 10^{-3} M) electrolyte concentrations. Heparin, a negatively charged polyelectrolyte, was adsorbed to the pore wall to augment electrostatic effects. The data were compared with numerical calculations based on a diffuse double-layer model, and the unknown pore wall charge densities were computed for each experiment. The results show that the classical analysis is somehow deficient and also that adsorption of the potential determining ion (heparin) is dependent on electrostatic potential at the pore wall.

WEI-HU KOH
and
JOHN L. ANDERSON
School of Chemical Engineering
Cornell University
Ithaca, New York 14853

SCOPE

It has long been known that momentum and ion transport are coupled in fluid systems not locally constrained by electroneutrality. The existence of a nonzero space charge provides the coupling mechanism in two ways. First, its interaction with an applied (dynamic) electric field generates a body force in the momentum balance, and, second, the large magnitude of the electrostatic potential in the space charge region causes counterion enhancement and coion exclusion (Donnan effect). Because of physical limitations on charge separation, regions of space charge are confined to the proximity of charged interfaces; the space charge-interface composite is known as the electrical *double layer*. Interactions between double layer and transport driving forces directed parallel to the interface result in the so-called *electrokinetic phenomena* (Davies and Rideal, 1961; Adamson, 1967), common examples of which are electroosmosis, volume flow past a stationary interface resulting from an applied electric field parallel to that interface; streaming potential, the generation of parallel voltage difference from a pressure driven flow; electrophoresis, migration of a charged interface (particle) in an applied electric field; and enhanced conduction or surface conduction, augmentation of ion fluxes (or specific conductivity) in an applied electric field. Some of these effects are quite strong, and their importance generally increases to the point of dominating the transport as the interfacial area per fluid volume becomes large.

Because of their direct relationship to double-layer structure (ion and potential distribution), measurable electrokinetic phenomena have long been used to characterize the double layer (for example, zeta potential). There are pitfalls in such an approach, however, since rigorous experimental confirmation of the classical double-layer model (Gouy-Chapman) is lacking, and the geometries of most experimental systems (usually microporous media) are quite complex, differing substantially from the relatively simple ones used in mathematical analyses. Essentially the problem has been one of too many physical unknowns (geometry, charge density, etc.) and too few independent experiments.

Of interest in this work is electroosmosis and enhanced conduction in small, highly charged microcapillaries. The formulism for circular pores is developed in the literature (Dresner, 1963, 1965; Morrison and Osterle, 1965; Fair and Osterle, 1971; Jacazio et al., 1972) and is based on the diffuse double-layer model (Verwey and Overbeek, 1948; Overbeek, 1952). If the pore is very long, the ion distribution in the double layer extending perpendicular from the pore wall toward the center is assumed to be in an equilibrium state, thereby uncoupling the mathematics for radial ion distributions (Poisson-Boltzmann equation) from those for axial transport rates if the pore connects two solutions of equivalent ionic strengths. In electroosmosis experiments a volume flow through the pores is measured as a function of applied potential difference (or electrical current) across the membrane, while enhanced conduction involves measurement of the current-applied voltage characteristics of the membrane. These two phenomena are independent in a phenomenological sense, and hence each provides an independent measure of double-layer properties.

Electroosmotic flow and pore solution conductivity were measured in well-defined microcapillaries over a range of pore dimensions and electrolyte (potassium chloride) concentrations. An important aspect of the experiments was that the range of pore radii examined was of order equal to the Debye length parameters for moderate electrolyte concentrations, so that a large percentage of pore solution was under direct influence of the counterion space charge. Numerical solutions to the Poisson-Boltzmann and modified Navier-Stokes equations were compared to the data for a particular pore radius and electrolyte concentration to obtain two estimates of charge density at the pore wall, which was augmented by adsorption of heparin. Consistency of these estimates was used as a criterion for evaluating the success of the classical analysis, and variations of wall charge with electrolyte concentration were interpreted physically to mean that the extent of heparin adsorption is a function of the electrostatic potential at the pore wall.

CONCLUSIONS AND SIGNIFICANCE

Numerical solutions to the equilibrium double-layer and transport equations were obtained for both circular and elliptical (eccentricity = 2.5) pores. For the electrolyte potassium chloride which is symmetric in both charge number and ion mobility, the observable variables are only a function of (r_o/L) and $(r_o\sigma)$, where r_o is the radius of a circle of equivalent pore area, L the Debye length, and σ the charge density at the pore wall due to ion adsorption. The ratio of pore-to-bulk specific solution conductivity (enhanced conductivity) calculated from the classical model is nearly the same for pores of both shapes at the same parameter values, while the induced flow rate per applied electric field across the pore (electroosmotic flow coefficient) is quite sensitive to pore shape, being roughly 20 to 30% larger for circular pores.

Wall charge densities obtained from comparison of the numerical results with the data for enhanced conduction and electroosmosis at identical physical conditions did not agree and in some cases differed by a factor of 5. These discrepancies were taken as evidence that a basic flaw exists in the classical theory for the double-layer and associated electrokinetic phenomena. Although the Gouy-Chapman model itself has been examined theoretically and found adequate for most conditions (Bolt, 1955; Levine and Bell, 1966), the anomalies due to a nonuniform charge distribution on the pore wall, which could conceivably have occurred in our pores owing to uneven heparin adsorption, have received little attention in the literature.

For small values of r_o/L, solution within the pores displayed a specific conductivity approaching 100 times that of the bulk solution, while flow rates induced by an applied electrical potential of 1V across pores ~300Å radius were equivalent to those induced by a pressure difference of order 10 atm. However, these electrical effects on transport were still not as large as anticipated from charge densities estimated for heparin adsorption to the basal surface (faces) of mica (Stoner et al., 1971). The amount of heparin adsorbed to the pore wall was found to increase with electrolyte concentration and could be correlated with the calculated electrostatic potential at the pore wall. Further evidence of unsaturation was demonstrated by an observed increase in apparent wall charge when the heparin concentration in the bulk solution was doubled.

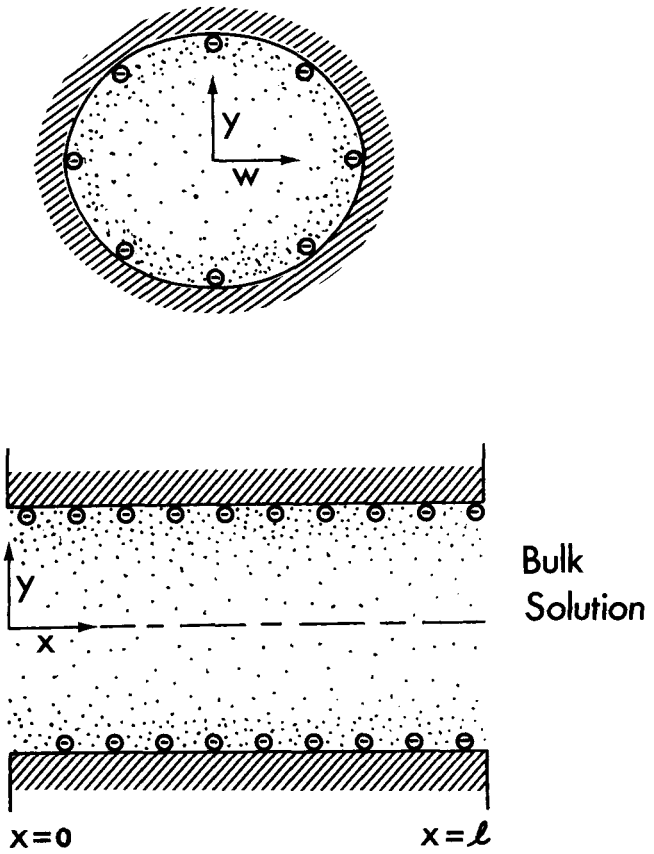

Fig. 1. End and side view of the model pore. The negative polyelectrolyte heparin is shown tightly adsorbed to the pore wall. The space charge density is represented by the intensity of the black dots.

Emanating from a charged interface into the adjacent electrolyte solution is a region of nonuniformly distributed space charge of opposite sign as shown in Figure 1. The total charge of the interface plus solution (or the double layer) cancel to adhere to the principle of electroneutrality.

The importance of the double layer is greatest in systems with very large surface area, so it is not surprising that much of the literature is concentrated in the area of colloid science (Verwey and Overbeek, 1948; Overbeek, 1952) and electrochemistry (Grahame, 1947; Frumkin, 1960; Newman, 1973). Helmholtz (1853) is given credit as the first to properly include the electrodynamic body force term in the momentum equation for a liquid, and his equation still finds popular use today. The literature on the equilibrium double layer and its effect on transport processes is prodigious, and extensive reviews are available (for example, Davies and Rideal, 1961; Adamson, 1967; Dukhin and Derjaguin, 1974).

The basic structure of the space charge region of the equilibrium double layer was formulated independently by Gouy and Chapman 65 yr. ago. This particular model goes by their name as well as the diffuse double layer. The essential features are: (1) counterions (ions of sign opposite to the surface charge) are attracted to the surface by coulombic forces while coions are repelled; (2) all ions in solution resist accumulation at any point because of Brownian motion; and (3) Poisson's equation relates the spatial variation of potential to space charge density such that accumulation of space charge tends to reduce in magnitude the electrostatic potential throughout a continuous medium. A statement of (1) and (2) is the Boltzmann equation which relates point differences in ion concentration to differences in electrostatic potential at equilibrium conditions. For various reasons, the diffuse model is only valid for solutions of low ($\lesssim$ 0.1 M) ionic strength and at distances at least two or three ionic diameters from the interface (Onsager, 1933; Bolt, 1955; Levine and Bell, 1966; Sparnaay, 1972; Reeves, 1974). In concentrated solutions of electrolytes, self-atmosphere ion-ion interactions become important, and very near the charged interface ion dimensions and solvation characteristics are factors. A good qualitative discussion of possible flaws in the classical diffuse model is given by Davies and Rideal (1961).

Stern (1924) proposed the existence of a region adjacent to the charged interface where ions are very tightly bound electrostatically as well as (perhaps) by intermolecular forces. The nominal purpose of this postulate was to account for finite ion dimensions and ion specificity; furthermore, such a model would eliminate calculations predicting impossibly large counterion concentrations near the interface as sometimes result from using the diffuse theory equations. Grahame (1947) assigned a structure to this region postulating the existence of inner and outer "Helmholtz planes," the former representing the closest approach of the centers of counterions and the latter the closest approach of coions. At high potentials, the counterions at the inner Helmholtz plane may be adsorbed and relatively immobile, perhaps even establishing a discrete charge effect (Levine et al., 1972). The thickness of the Stern layer is often estimated as 2 to 4 Å (to the outer Helmholtz plane), and the diffuse model is assumed valid outside this region. It has also been proposed that dielectric saturation (that is, a depressed dielectric constant for the solvent due to a high electric field) be incorporated in the Stern model (Grahame, 1950; Conway et al., 1951; Booth, 1951; Buckingham, 1956), but quantitative aspects of such treatments seem arbitrary. There does not appear to be an accepted quantitative model of the Stern layer, and hence its role in double-layer theory has in part become one of providing a source of adjustable parameters to aid in interpretation of experimental results. A general rule of thumb says that the Stern layer loses its physical importance in systems where the Debye length parameter [Equation (7)] is at least an order of magnitude larger than ionic dimensions, and counterion concentrations near the interface remain reasonably small.

Our purpose in these experiments was to carefully examine certain transport processes in small, charged capillaries. A system of well-defined pores was achieved by using track etched mica as the porous septum. To enhance electrostatic effects on transport as well as to provide limited control on charge densities within the pores, the negative polyelectrolyte heparin was added to the solutions with the expectation that it would irreversibly adsorb to the pore wall (Stoner et al., 1971). Membranes were fabricated with pore radii comparable to the solution Debye length parameter, thereby allowing us to investigate quantitatively processes in pores whose interior was charged throughout even at moderate concentrations of supporting electrolyte. All pore geometric parameters were known a priori; so the only unknown parameter in each experiment was the pore wall charge density (σ) resulting from the adsorption of heparin.

The experimental strategy was to measure two independent* electrokinetic parameters, enhanced conduction (or surface conduction, Rutgers and de Smet, 1947) and elec-

* These two processes are not cross related and hence not subject to the Onsager reciprocal relationship.

troosmotic flow, over a range of pore radii (150 to 600 Å) and electrolyte concentrations (KCl, 10^{-4}-10^{-1} M). Our control over pore numbers and dimensions permitted the experiments on enhanced conduction, for with most membranes the resistance is smaller than that of the bulk solutions on each side, and increases in membrane conductivity cannot be directly observed (Mackay and Meares, 1959). In order to obtain two independent estimates of pore wall charge at each condition, σ was calculated from these data with the help of numerical solutions to the double-layer and one-dimensional transport equations based on the Guoy-Chapman model. A critical test for the validity of this classical model is whether or not the two independent estimates of σ agree at each pore radius and electrolyte concentration. Our efforts were directed entirely at evaluating the validity of the classical model rather than elucidating the actual deficiencies. Of additional interest was the manner in which adsorption of the potential determining ion (heparin) is affected by supporting electrolyte concentration, since it is this type of adsorption which essentially determines the electrostatic effects on equilibrium ion distributions and transport processes within small pores.

ANALYSIS OF PORE TRANSPORT

The model pore (Figure 1) is a long, cylindrical capillary of arbitrary shape which connects two infinite reservoirs containing identical solutions of a single electrolyte. The pore radius (r_o) is defined as the radius of a circle with area equivalent to the actual pore. The basic equations describing electrohydrodynamics of a Newtonian liquid whose viscosity may change at high electric fields (Andrade and Dadd, 1951) at low Reynolds numbers and steady conditions are (Melcher and Taylor, 1969).

$$\vec{\nabla} \cdot (\eta \vec{\nabla} \vec{U}) = \vec{\nabla} P + \rho_e \vec{\nabla} \Phi - \frac{1}{8\pi} \left(\rho \frac{\partial \epsilon}{\partial \rho} \right) \vec{\nabla} (\vec{\nabla} \Phi)^2 + \frac{1}{8\pi} (\vec{\nabla} \Phi)^2 \vec{\nabla} \epsilon \quad (1)$$

$$\vec{\nabla} \cdot (\epsilon \vec{\nabla} \Phi) = -4\pi \rho_e \quad (2)$$

where Φ is the total electrical potential, ρ_e is the fluid space charge density, and ϵ, η, and ρ are the fluid dielectric constant, viscosity, and density. Equation (2) is the Poisson equation and may be incorporated directly into (1) to eliminate ρ_e. The third term on the right-hand side of (1) is called *electrostriction* and has the effect of enhancing the stress normal to charged interfaces (Babchin, 1974). The fourth term represents a polarization effect and is usually neglected ($\epsilon \doteq$ constant), although at very large electric fields it may be important.

The pore length-to-radius ratio (l/r_o) is assumed quite large, so that momentum and ion fluxes are one dimensional in the axial (x) direction. Also, the charge adsorbed to the pore wall is assumed uniform (the so-called *smear charge* assumption, Frumkin, 1960) and immobile with respect to ion transport. The mathematically convenient result is that the electrostatic (double-layer) and trasport equations become sequentially coupled, with the former being independent of any transport rates. The total potential is decomposed into an electrostatic contribution ϕ and a dynamic (or applied) contribution V:

$$\Phi = \phi(w, y) + V(x) \quad (3)$$

with (w, y) representing the radial coordinates in the pore cross section and x the axial coordinate. The electrostatic contribution is only a function of (w, y) because the bulk solutions at either end of the pore have identical electrolyte concentrations [for the asymmetric case, when $\phi = \phi(w, y, x)$, see Fair and Osterle, 1971]. Since there is no transport radially within the pore, the principles of conservation of mass ($\partial U_x/\partial x = 0$) and charge ($\partial i_x/\partial x = 0$) require that $V'(x)$ be a constant as seen in Equation (12).

The diffuse double-layer equation is developed from both the Poisson equation (by assuming constant dielectric properties) and the Boltzmann relation. The latter derives from radial equilibrium within the pore by assuming unit activity coefficients:

$$C_\pm = C_{\pm\infty} \exp\left[\frac{-z_\pm e\phi}{kT} \right] \quad (4)$$

The subscript ∞ denotes bulk solution outside the pore, where $\phi = 0$. The space charge is simply the sum of the ionic charge concentrations at any point:

$$\rho_e = N_o e [z_+ C_+ + z_- C_-] \quad (5)$$

For a symmetric electrolyte, $z_+ = -z_- = z$. Combination of Equations (2) to (5) yields the classical Poisson-Boltzmann equation which is used to describe the equilibrium diffuse double layer:

$$\nabla^2_{wy} \Psi = \frac{1}{L^2} \sinh(\Psi) \quad \left(\Psi \equiv \frac{ze\phi}{kT} \right) \quad (6)$$

$$L \equiv \left[\frac{\epsilon kT}{8\pi N_o e^2 z^2 C_\infty} \right]^{1/2} \quad (7)$$

The parameter L is called the *Debye length* and is often used as the characteristic thickness of the double layer. Conservation of charge must be realized so that the total charge in the pore fluid is equal in magnitude but opposite in sign to the fixed charge at the pore wall. An integral statement of this restraint, by using Equation (2) and the divergence theorem, leads to the proper boundary condition for Equation (6):

$$\text{pore wall:} \quad \vec{n} \cdot \vec{\nabla}_{wy} \Psi = \left(\frac{4\pi ze}{\epsilon kT} \right) \sigma \quad (8)$$

$\vec{n}$ is the unit normal vector pointing outward from the pore wall, and σ the fixed charge density (esu/cm^2) at the pore wall. Notice that Equations (6) to (8) are independent of any transport equation but still contain one unspecified parameter (σ).

The axial momentum transport relation derives from Equation (1) by assuming constant viscosity:

$$\eta \nabla^2_{wy} U_x = \frac{\partial P}{\partial x} - 2N_o ze C_\infty \sinh(\Psi) V'(x) \quad (9)$$

where U_x denotes the axial point velocity and Equations (2) to (5) have been used to eliminate the space charge density. Mass continuity requires U_x to be independent of x. Owing to mechanical equilibrium, the pressure is a function of all three coordinates, but the radial dependence is only related to the electrostatic potential profile; thus, the pressure is the sum of two contributions:

$$P = P_1(w, y) + P_\infty(x) \quad (10)$$

P_1 is easily computed (Babchin, 1974) but has no influence on axial transport rates.* If there is no applied pressure difference across the membrane, then $P_\infty'(x) = 0$ and

* If the capillary connects two reservoirs of dissimilar electrolyte solutions, then this pressure representation is invalid (Fair and Osterle, 1971).

the axial momentum equation reduces to

$$\eta \nabla^2_{wy} U_x = - [2N_o zeC_\infty] \sinh(\Psi) V'(x) \qquad (11)$$

$$\text{pore wall:} \quad U_x = 0$$

If $\Psi(w, y)$ is known from solution of Equations (6) and (8), the above linear equation can be solved numerically.

The second transport equation pertains to the point current density:

$$i_x = - (\kappa_+ + \kappa_-) V'(x) + \rho_e U_x \qquad (12)$$

The specific ion conductances (κ) are approximately proportional to ion mobility and concentration. It is assumed that both ions have the same mobility (for example, potassium chloride). By using (2) to (5), Equation (12) is rewritten as

$$i_x = \kappa_\infty \cosh(\Psi)(- V'(x)) - [2N_o zeC_\infty] \sinh(\Psi) U_x \qquad (13)$$

The first term on the right is a migration contribution to the local current density, while the second term represents convective transport. Outside the double layer local electroneutrality exists ($\Psi = 0$), and the convective part is zero. The current density is readily computed if $\Psi(w, y)$ and $U_x(w, y)$ are known.

Calculations of local values of fluid velocity and current density are made by solving Equations (6) to (8), (11), and (13) in that order. Of interest physically are the measurable flow and current:

$$\langle U_x \rangle = \frac{1}{A_p} \int\int_{A_p} U_x \, dA \qquad (13)$$

$$\langle i_x \rangle = \frac{1}{A_p} \int\int_{A_p} i_x \, dA \qquad (14)$$

The electroosmotic coefficient (α) is defined as the average pore velocity per unit applied electric field:

$$\alpha \equiv \frac{\langle U_x \rangle}{- V'(x)} \qquad (15)$$

The enhanced conductivity (β) of the pore solution is defined as the average current through the pore divided by the current (i_∞) expected if there were no double layer in the pore ($\Psi = 0$):

$$\beta \equiv \frac{\langle i_x \rangle}{i_\infty} = \langle \cosh(\Psi) \rangle + \frac{[2N_o zeC_\infty]}{\kappa_\infty V'(x)} \langle U_x \sinh(\Psi) \rangle \qquad (16)$$

According to the classical theory presented above, these electrokinetic parameters should be functions of the fixed charge at the pore wall (σ), the pore geometry and size, electrolyte properties (κ_∞), and solvent properties (η, ϵ). In this work the usual assumption that η and ϵ have their normal bulk solution values is made. For capillary pores of arbitrary shape, the dimension of the cross section (r_o) is defined as the radius of a circle of equivalent area. Two pore shapes are considered: a circle and an ellipse. The shape of the ellipse is characterized by the major-to-minor axis ratio which equals $[\tanh(\xi_o)]^{-1}$, where ξ_o is the radial elliptical coordinate of the pore wall (Happel and Brenner, 1965). The value $\xi_o = 0.4147$ is used here because this particular ellipse has the same perimeter/area ratio as the experimental pores ($\sim$ rhombus with angles 60 and 120 deg.).

Details of the mathematical methods are presented in the Appendix. For a given pore shape three parameters are considered: r_o, L (that is, bulk electrolyte concentration C_∞), and σ. For most salts the approximation $\kappa_\infty \doteq \lambda C_\infty$ is valid, where λ is a constant specific to the electrolyte of interest, and C_∞/κ_∞ is then eliminated from the second term in Equation (16). Nondimensionalization of the double-layer and transport equations shows that if pore shape, solvent, and electrolyte properties are chosen, then α and β depend solely on two parameter groups:

$$r_o/L \quad \text{and} \quad K \equiv \left[\frac{4\pi ze}{\epsilon kT}\right] r_o \sigma.$$

The parameter r_o/L is a measure of double-layer overlap within the pore, while K is proportional to the total wall charge per unit pore length.

EXPERIMENT

Porous membranes were made from thin ($\sim$ 7 μ m) sheets of muscovite mica by the track etch process (Quinn et al., 1972). First, the sheets were cut into circular disks 5.5 cm in diameter which were weighed to determine the thickness. The disks were then placed in a small irradiation cell where they were bombarded under controlled conditions with heavy fission fragments emitted by a small Cf^{252} source. The area subject to bombardment was a concentric circle of radius 0.8 cm. Each fission fragment impinging on the mica created a damaged track from which a pore was formed by etching in aqueous hydrofluoric acid. The irradiation time was carefully controlled, and since the fission process was random, the time was proportional to the number of pores in the membrane; the proportionality constant was known from optical calibrations. The pore dimension was controlled by the etching time.

A particular advantage of mica membranes was that each membrane could be characterized absolutely with regard to pore geometry. Since all pores were perpendicular to the mica sheet (this was ensured by alignment in the irradiation chamber), the pore length (l) was identically equal to the membrane thickness. The number of pores (n) was calculated from the irradiation time. Finally, the effective pore radius was determined by measuring the electrical d.c. resistance of the membrane in concentrated (> 0.1 M) potassium chloride solution:

$$R = \frac{\Delta V}{I} = \frac{l}{\kappa_\infty (n\pi r_o^2)} \qquad (17)$$

At such high salt concentrations enhanced conductivity effects were negligible; furthermore, the charge on the pore wall was small, since heparin was purposely omitted from the salt solutions used to measure pore radius. By this resistance measurement we were essentially measuring the area of each pore (πr_o^2).

The physical characteristics of mica membranes justify the label "model membranes." Besides the ability to independently control and measure each of the geometric properties (l, n, r_o), all pores in any one membrane have very nearly the same radius and do not intersect with each other. The pores are true capillaries of near molecular and colloidal dimension (r_o may be varied from 30 Å to several μ m). Therefore, no adjustable geometric parameters such as tortuosity factor are required, and basic phenomenological relationships postulated for microporous transport may be tested without compromise of a one-to-one relationship between mathematical model and physical characteristics. There is one undesirable characteristic of mica membranes: the cross section of the pores is a 60 deg. rhombus rather than a circle. To account for this shape the pores are assumed to be elliptical, with an eccentricity giving the same perimeter/area ratio as the rhombus. We feel that there are no sharp corners in the smaller (< 0.1 μ m)

pores, and hence an ellipse is a good physical representation; furthermore, the mathematics are simplified from a numerical viewpoint, since elliptical coordinates are orthogonal.

The membrane cell is shown in Figure 2 and was constructed of Plexiglas®. For the enhanced conductivity experiments, a double-pair reversible electrode (silver/silver chloride) arrangement was used to eliminate electrode overpotential at the voltage sensing electrodes (inner pair). A constant d.c. current from a Keithley model 225 current source was transmitted through the outer electrode pair. The current direction was reversed every few seconds to check for polarization effects (which were never found to exist). Stirring was utilized to prevent charge polarization at the membrane-solution interfaces. The transmembrane potential was measured by a Keithley model 602 electrometer. The membrane pore area was kept small enough so that the bulk solution resistance on either side was negligible compared to the membrane resistance. For all experiments the current-voltage relationship of the membranes was linear. The pore solution specific conductivity was then determined from Equation (17) and the measured resistance (R):

$$\langle\kappa\rangle = \frac{l}{R(n\pi r_o^2)}$$

The enhanced conductivity ratio was computed as $\beta = \langle\kappa\rangle/\kappa_\infty$.

The same cell was used for the electroosmotic flow measurements at zero pressure difference as shown in Figure 3. A known constant d.c. current was forced through a single pair of electrodes and the membrane. Two nearly horizontal pipettes, one fixed to each side of the membrane, showed the volume change per time due to electroosmotic flow. The volume flow always occurred toward the cathode side of the cell, thus confirming that the charge on the pore wall was negative. To prevent slight deflections the membrane was supported by Plexiglas disks with a concentric hole exposing the transport area of the membranes. The system was leak tested to our satisfaction, and in all experiments material balances from both pipettes were excellent. The volume flows generated were found to be quite stable and linear with current through the membrane. Flow rates of the order 70 μ l/hr. were measured. Figure 4 illustrates typical transport rates.

In the enhanced conductivity experiments a very small pore area (that is, small number of pores) was desirable, since the membranes were so thin and the bulk phase resistance was to be kept negligibly small in comparison to the membrane resistance. (In fact, our ability to tailor the number of pores allowed this measurement. Very few enhanced conductivity measurements have been reported in the literature for this reason.) However, for the electroosmosis experiments a large pore area was needed to obtain appreciable volume flows across the membrane. It was impossible to perform both experiments on the same membrane and maintain sufficient accuracy, so that a different membrane was used for electroosmosis than for enhanced conductivity. It is emphasized, however, that the only difference between the two membranes was the number of pores. Both membranes were equal within 10% in thickness (the thickness of each membrane was known to be within $\pm$ 1%), and both were etched in the same hydrofluoric acid bath to ensure identical pore dimensions. Since calculations and experimental tests confirmed that adsorption of electrolyte was not a factor even for potassium chloride concentrations as low as 10^{-4} M, the number of pores was a trivial difference between the membranes from a phenomenological viewpoint. Table 1 lists the pertinent characteristics of the membranes (A series for enhanced conductivity, B series for electroosmosis).

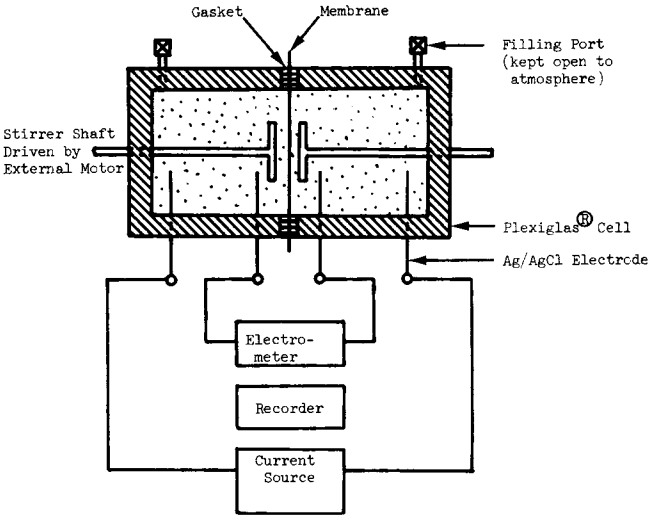

Fig. 2. Apparatus for pore conductivity experiments. Small dots represent electrolyte solution (not space charge).

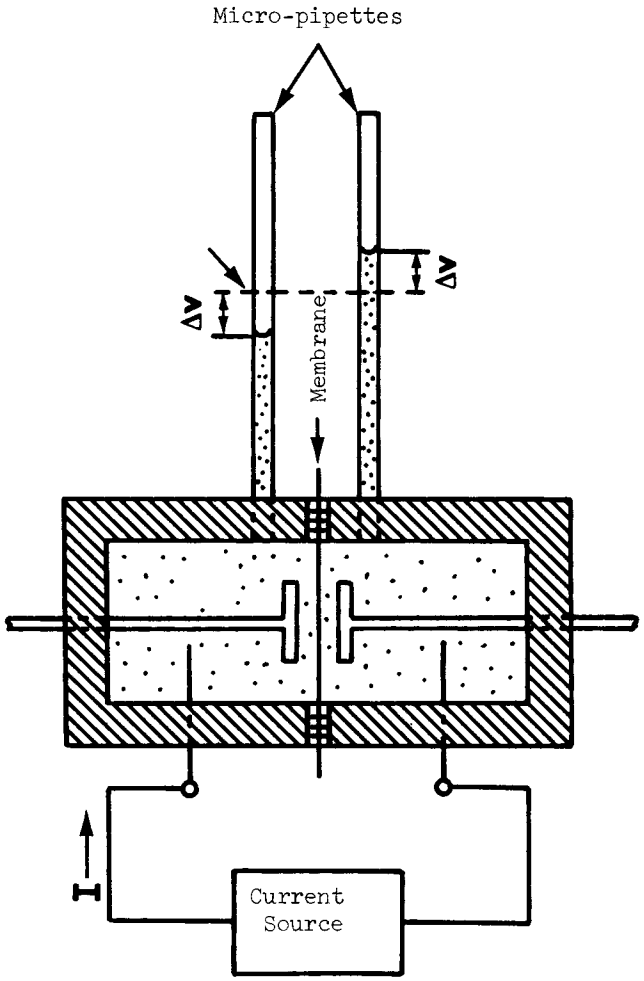

Fig. 3. Apparatus for electroosmotic flow experiments. A Plexiglas® support piece (not shown) was positioned on the cathode side to prevent membrane deflection. Evaporation rates from the micropipettes were found to be negligibly small. The micropipettes were positioned horizontally.

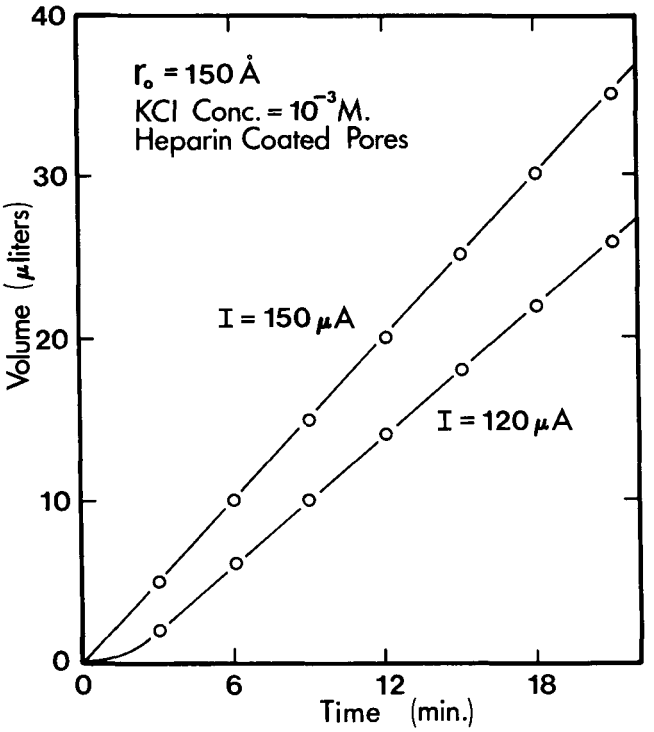

Fig. 4. Sample flow rate data. The lag period for the smaller current was observed in several experiments and is quite common in the existing literature. This lag cannot be attributed to any apparent time constant for the membrane and may be the result of slight membrane deflections.

TABLE 1. CHARACTERISTICS OF THE TRACK ETCHED MICA MEMBRANES USED IN THE EXPERIMENTS. PORE RADIUS (r_o) IS BASED ON A CIRCLE OF AREA EQUIVALENT TO THAT OF THE ACTUAL RHOMBUS SHAPED PORES. THE MEMBRANE CELL CONSTANT (K_o) IS DEFINED AS THE PORE LENGTH (MEMBRANE THICKNESS, l) DIVIDED BY THE TOTAL PORE AREA. A SERIES MEMBRANES WERE USED IN THE CONDUCTION EXPERIMENTS, B SERIES FOR ELECTROOSMOSIS

Membrane	$l \times 10^4$, cm	r_o, Å	K_o, cm^{-1}
A-1	6.86	150	388
B-1	7.04	150	≈1
A-2	7.65	310	292
B-2	7.01	310	≈1
A-3	7.28	570	152
B-3	7.71	570	≈1
A-4	7.19	210	470
A-5	7.53	120	583

The salt solutions were made from sterile, low conductivity water (Milli-Q2® system, Millipore Corporation, Bedford, Mass.) and reagent grade potassium chloride. The range of salt concentration was 10^{-4} to 2×10^{-1} M, corresponding to Debye lengths of 304 to 6.8 Å. In all but one set of experiments the polyelectrolyte heparin was added for the purpose of maintaining a high charge density at the pore wall. Heparin polymers have a charge of −6e/940 atomic mass units. In all such solutions the heparin was USP grade and at a constant concentration of 1 unit/cm^3 (1 unit = 6.25 mgm), and solution pH was ≈ 6 to 7.

The bulk conductivities (κ_∞) of all solutions were determined with a standard Leeds and Northrup cell and null bridge and were found to equal the literature value (Weast, 1971) for the nominal potassium chloride concentration except at 10^{-4} potassium chloride, for which the measured κ_∞ exceeded the literature value by 5 to 10% due to the heparin and its counterions. In all instances the measured value was used as the bulk conductivity in the analyses.

In both the enhanced conductivity and electroosmotic flow experiments the membrane (A or B series) was clamped into the cell and the cell filled with the most concentrated potassium chloride solution. (With the A series membranes, however, the pore radius was first determined by measuring the membrane resistance, as described before, by using 0.1 to 1.0 M salt solutions without heparin.) After about 30 min. the measurement was made; the enhanced conductivity determination required 5 to 10 min. at most, while electroosmotic flow required 1 to 2 hr. The solution in the cell was then removed, the cell rinsed thoroughly and then filled with the next less concentrated potassium chloride solution. Between solution changes in the cell, at least 15 min. were allowed for equilibration. After the measurement on the most dilute potassium chloride solution, the procedure was reversed (from dilute to concentrated). No hysteresis was ever observed in either the enhanced conductivity or the electroosmotic flow measurements. The purpose in selecting the direction concentrated to dilute salt solutions on the first leg was to reduce the electrostatic effects on the rate of adsorption of heparin. It is emphasized that all salt solutions contained the same heparin per volume except in one set of experiments on membrane A-4 in which the heparin concentration was doubled for the purpose of investigating the degree of adsorption saturation.

A few enhanced conduction experiments were run without heparin on a membrane (A-5) of pore size 120 Å to study the double layer resulting from a natural charge on muscovite mica. The pH was adjusted to 7 and 9 by using potassium hydroxide and found to be stable over the short time necessary for the experiments.

The experimental error should be small based on both estimates and reproducibility. The uncertainty in κ is ±5% (reproducibility usually ±2% for a single membrane) and in Q/I is ±5%. Thus, the uncertainty in α is ±7% in most cases. Owing to problems with the californium source, the estimated pore number (n) could be in error by ±10% (note, however, that the experimental determination of κ/κ_∞ and Q/I was independent of n), and since the estimate of r_o depends on $n^{1/2}$, the uncertainty in r_o in Table 1 and Figures 5 and 6 is ±5%.

RESULTS AND DISCUSSION

The numerical calculations (see Appendix) for enhanced pore conductivity (β) and electroosmotic flow coefficient (α) are plotted in Figures 5 and 6. In the experiments all dimensionless potentials (Ψ) and charge densities (σ) were negative, but because the electrolyte is symmetric in charge and mobility, the calculations for $+\sigma$ are identical in magnitude to those for $-\sigma$ (except for the sign of U_x). Hence, all charges and potentials are expressed as magnitudes with the understanding that they are negative in sign. The abscissa is r_o/L which can be interpreted as the equivalent pore radius divided by the characteristic double-layer dimension. For a pore of constant dimension, increases in r_o/L translate into increases in $C_x^{1/2}$; as more electrolyte is added, the abscissa increases and less of the pore fluid is charged. The parameter K is a measure of total wall charge ($r_o\sigma$) for a pore of constant dimension.

An increase in pore dimension results in a proportional increase in r_o/L and K.

Several rather interesting characteristics of the electrokinetic plots are immediately discernible. Calculations for enhanced conductivity in a circular capillary vs. an elliptical one are nearly identical for equivalent areas. This result is somewhat encouraging, since it supports the practice of using circular cross sections (which are desirable mathematically) in modeling arbitrary pore geometries of a capillary nature. Unfortunately, Figure 6 indicates that significant differences in electroosmosis are expected depending on the shape of the pore. The ellipse offers a higher resistance to flow, probably because of the larger pore wall area per liquid volume.

For $r_o/L \lesssim 1$, the electroosmosis coefficient becomes independent of r_o/L. In the limit as $r_o/L \to \infty$, all capillary geometries converge to the Helmholtz limit for thin double layers:

$$\alpha = -\left[\frac{\epsilon kT}{4\pi ze\eta}\right]\Psi_w \tag{18}$$

$$\Psi_w = 2\sinh^{-1}\left[\frac{1}{2}\,\frac{K}{(r_o/L)}\right] \tag{19}$$

Equation (19) is the potential-charge relationship for a flat plate in an infinite liquid phase (Adamson, 1967). [As an aside, the results of our numerical calculations show that Equation (19) is a reasonably good, general approximation of the charge-potential relation for both circular and elliptical pores at all r_o/L. This result was unexpected but quite useful.] The Helmholtz model considers the double-layer region to be very thin compared to the radius of curvature of the pore wall, so the velocity profile appears to be a plug flow. It is noted that although some prefer to call the electroosmotic flow in large pores a *slip* flow, the no-slip boundary condition at the pore wall is explicitly used in the Helmholtz derivation.

A brief discussion of two often used electrokinetic concepts is necessary to avoid confusion. The *zeta potential* is usually defined as the electrostatic potential at the shear plane in the liquid adjacent to a charged solid surface. To maintain consistency with the continuum hydrodynamic approach, the shear plane should be assumed to be the actual solid/liquid interface,* so that zeta potential in our model pores is identified with the electrostatic potential at the pore wall (Ψ_w) which is a function of charge density, pore radius, and Debye length. *Donnan exclusion* is a concept usually referring to complete exclusion of coions from pore solution. Although this is never exactly true, coion concentrations are practically negligible for conditions when $\Psi > 1$ for all positions inside the pore. An assumption often used with the Donnan concept is that electrostatic potential and hence space-charge density are independent of position in the pore (sometimes termed *fixed charge* or TMS theory, Hoffer and Kedem, 1972). Such an assumption can be shown to be correct only for very small pores by considering a circular capillary in the high potential limit described by Equation (A3) in the Appendix. Since charge density is proportional to exp (Ψ) when coions are excluded, the ratio of space charge at the pore wall to that at the pore center is given by the following under the restraint of Equation (A4):

$$\frac{\rho_e(1)}{\rho_e(0)} = 1 + \left(\frac{K}{4}\right)^2 \tag{20}$$

* Location of the shear plane provides the experimenter with one more adjustable parameter with which to maneuver. Its concept, however, lacks physical rigor.

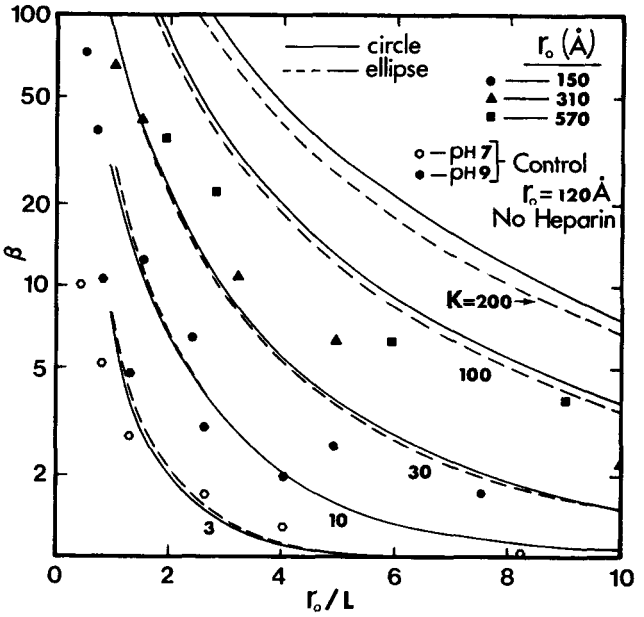

Fig. 5. Ratio of pore-to-bulk specific conductivity (β) vs. dimensionless pore radius. r_o is based on a pore of equivalent circular area. The parameter K is proportional to $r_o\sigma$. For all membranes except the control, the bulk electrolyte (potassium chloride) solution contained 1 unit heparin/ml.

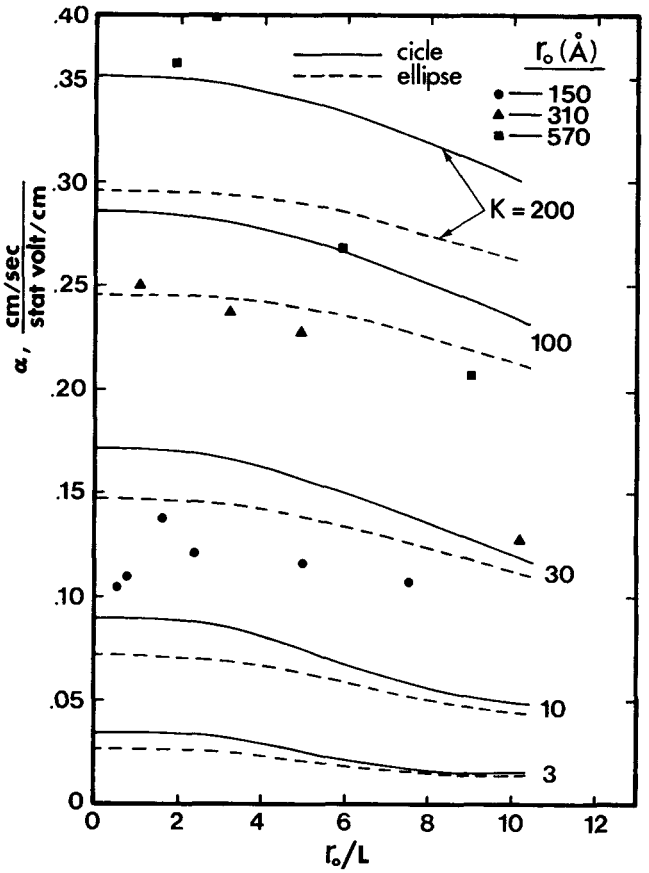

Fig. 6. Electroosmotic flow coefficient (α) vs. dimensionless pore radius. All bulk solutions contained heparin at 1 unit/ml. α was calculated from $\kappa Q/I$, where Q/I was measured, and κ (pore solution specific conductivity) was determined from the conduction experiments (data shown in Figure 5).

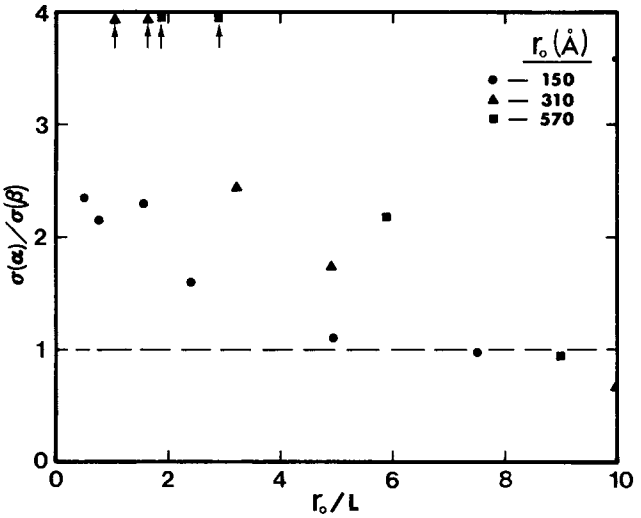

Fig. 7. Ratio of pore wall charge deduced from electroosmosis [$\sigma(\alpha)$] to charge deduced from conduction [$\sigma(\beta)$] vs. dimensionless pore radius. Arrows indicate that the datum point is above an ordinate value of 4.

As will be seen from our experimental results, K may range from 10 to 100 for pores 150 to 570 Å in radius, so that space charge is highly nonuniform even when coions are excluded from the pore solution. Thus, proper use of the fixed-charge theory of ion distribution demands careful inspection of pore size, charge density, and Debye length.

The experimentally determined pore/bulk conductivity ratios are plotted in Figure 5. The control was run (r_o = 120 Å) without heparin for the purpose of assessing the natural charge on the mica wall. This charge was negative and *p*H dependent, and its magnitude appears to have increased with increasing salt concentration (decreasing L) and *p*H, which is consistent with the observations of Abendroth (1972) on clay suspensions. These data when compared to the heparin results demonstrate that heparin strongly enhanced the wall charge density.

The enhancement of pore solution conductivity at small values of r_o/L was large (of order ~ 100) in the heparin experiments but not as great as anticipated. Stoner et al. (1971) reported that heparin adsorption from 0.1 M salt solutions to mica surfaces approached compact monolayer densities. Such surface concentrations should yield charge densities of 6 to 12 × 10^4 esu/cm², while our results are considerably smaller (see Table 2). Stoner et al. also found the adsorption to be irreversible, which should have resulted in our data for any one pore size coinciding with or being parallel to an isocharge (constant K) curve in Figure 4; such behavior is definitely not observed. [It should be noted that the data would also fail to coincide with any isopotential curve were Ψ_w used as the parameter in place of K].

By using the numerical calculations and the known values of r_o/L, each measured value of β was used to interpolate for the unknown value of K, from which the pore wall-charge density was computed as well as the average dimensionless wall potential (Ψ_w). It is noted that in capillaries which are not circular, a constant σ does not produce a constant potential on the pore perimeter, although for an ellipse Ψ_w varies only slightly in most cases. The results for all heparin experiments as well as for the non-heparin control are listed in Table 2. A uniform trend of increasing wall charge with r_o/L is evident, which indicates that the extent of heparin adsorption was variable; furthermore, the magnitude of σ was a factor of 10 smaller than estimated by Stoner et al. Since there was no direct method of measuring wall charge, each determination cannot be evaluated by itself.

Table 2. Summary of Wall-Charge Density (σ) and Average Dimensionless Wall Potential (Ψ_w) Obtained by Comparison of the Conduction Data with Numerical Calculations Based on the Diffuse Double-Layer Model. All Electrolyte (Potassium Chloride) Solutions Contained 1 Unit/ml Except Those Used with the 120Å Pores (which Had No Heparin)

r_o, Å	r_o/L	$-\sigma \times 10^{-3}$, esu/cm²		$-\Psi_w$*	
150	0.49	2.6		5.6	
	0.75	3.0		5.2	
	1.56	4.1		4.4	
	2.37	4.8		3.8	
	4.94	7.0		3.0	
	7.49	8.6		2.7	
	15.61	10.5		1.9	
310	1.02	4.3		6.6	
	1.54	5.9		6.4	
	3.22	6.8		5.1	
	4.88	8.8		4.8	
	10.2	9.6		3.4	
	15.4	10.4		2.8	
570	1.87	4.1		6.4	
	2.84	5.9		6.2	
	5.91	6.7		5.1	
	8.97	8.5		4.6	
		*p*H7	*p*H9	*p*H7	*p*H9
120	0.40	0.3	—	3.5	—
(No heparin)	0.82	0.6	1.2	2.7	3.4
	1.27	0.9	1.5	2.0	3.0
	2.63	1.5	3.3	1.6	2.6
	4.01	2.2	4.2	1.4	2.2
	8.24	2.5	—	0.7	—

* $\Psi_w = \frac{ze\phi_w}{kT}$ at 25°C: $\frac{kT}{e}$ = 25.7 mV = 8.54 × 10^{-5} statvolts (z = 1 KCl).

Table 3. Summary of Wall Charge Density (σ) and Average Dimensionless Wall Potential (Ψ_w) Obtained by Comparison of Electroosmosis Data with Numerical Calculations Based on the Diffuse Double-Layer Model. All Electrolyte (Potassium Chloride) Solutions Contained 1 Heparin Unit/ml

r_o, Å	r_o/L	$-\sigma \times 10^3$, esu/cm²	$-\Psi_w$
150	0.49	6.1	6.9
	0.75	6.4	6.5
	1.56	9.5	5.9
	2.37	7.6	4.6
	4.94	7.9	3.2
	7.49	8.3	2.6
310	1.02	21.1	9.5
	1.56	>36	>9.4
	3.22	16.1	6.8
	4.88	15.2	5.8
	10.2	6.4	2.8
570	1.87	>21	>9.2
	2.84	>21	>8.3
	5.91	14.5	6.4
	8.97	8.0	4.6

The electroosmotic flow data are plotted in Figure 6. Since the measurements were of $Q/I = \langle U_x \rangle / \langle i_x \rangle$, it was necessary to multiply this ratio by the experimentally determined conductivity (κ) to obtain the coefficient α. These data do not coincide with a constant charge line for each pore size; in fact, they display a maximum near $r_o/L \sim 1$ which is unexpected from the analysis. Values for σ and Ψ_w interpolated from the electroosmosis data and numerical calculations for elliptical pores are listed in Table 3. Besides being greater in magnitude than the values determined from the conduction measurements, the deduced wall charge generally decreases as r_o/L increases, in contradistinction to the enhanced conduction results.

Although determination of the electroosmotic coefficient required knowledge of the pore conductivity, the two experiments were still independent. In Figure 7 is plotted the ratio of charge density determined from electroosmosis [$\sigma(\alpha)$] to that by conduction [$\sigma(\beta)$]. The fact that this ratio deviates so much from unity is indicative of a basic flaw in the electrokinetic double-layer model. A brief discussion of this conclusion is given later. For all three pore sizes this ratio decreases with increasing r_o/L, merely reflecting the opposite trends of $\sigma(\alpha)$ and $\sigma(\beta)$.

Enhanced pore conductivity seems to be a good kinetic parameter to measure wall charge for various reasons. The data are easily and quickly obtained. Because the membrane resistance is so large (small pore area), hydrodynamic and electrostatic effects in the bulk solutions on either side are definitely unimportant. The measured parameter (κ) is very sensitive to wall charge (or K), so that small errors in the former are not significant in interpolating for the latter, whereas the opposite is true of the electroosmotic coefficient. Finally, a circular pore can be used as a model for the real pores (elliptical) in the numerical calculations with little error. Most of the contribution to enhanced pore conductivity is the result of the equilibrium counterion distribution in the pore and as such may be more of a direct measure of the equilibrium double-layer structure than is electroosmosis which is totally dependent on the coupling between hydrodynamic forces and the double layer. In the following discussion it is assumed that the values of σ reported in Table 2 relate physically to the charge density at the pore wall.

Since the wall charge increased with r_o/L while potential decreased, the adsorption of heparin was probably reversible and perhaps a unique function of the potential at the pore wall. Equation (8) is one relation between charge and potential through an over-all electroneutrality condition, and hence one more relation between σ and Ψ_w is necessary to completely determine the system for given r_o and L. It is very common to find the subtle assumption that potential is constant with respect to electrolyte concentration, so that information at any one electrolyte concentration (or pore dimension, etc.) fully specifies the behavior of the system, but usually such an assumption is totally without justification. If a potential determining ion (for example, I^- for silver iodide sols, Verwey and Overbeek, 1948) is present in solution at a constant concentration, the constant potential assumption is thought to be valid, but our results show otherwise for the heparin/mica/potassium chloride system. (Heparin is the potential determining ion in that it adsorbs as a polyelectrolyte to the mica pore wall.)

Treatments of adsorption to solid/liquid interfaces generally ascribe a species-specific free energy of adsorption which appears in a Boltzmann form (Adamson, 1967). If the adsorbate is charged, an electrostatic term is usually added to the free energy of adsorption. By assuming that the nonelectrostatic energy contribution is constant, the equilibrium expression for a linear isotherm is

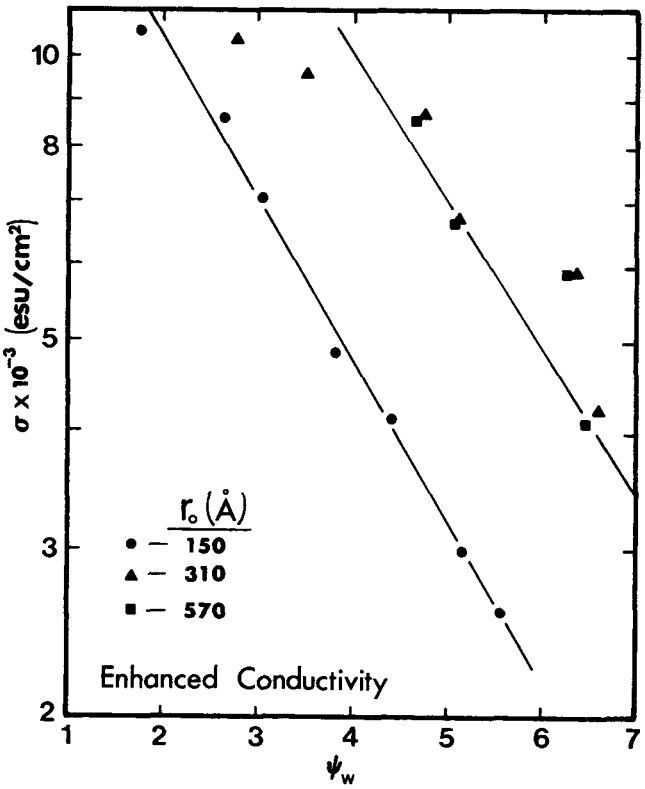

Fig. 8. Pore wall charge (σ) vs. average pore wall dimensionless potential (Ψ_w), both of which were deduced from conduction data. Only magnitudes are plotted; both charge and potential were actually negative in the system. The solid lines only help visual grouping of the data and are not physically significant. Although σ and Ψ_w are numerically related by Eq. (19), the absence of the parameter L results in this graph being a second independent relation between the two variables.

$$\sigma = \sigma_o \exp(-z^* \Psi_w) \tag{21}$$

where z^* is some type of effective charge number on the heparin molecule, and σ_o is the adsorbed density at zero potential which should be a function of heparin concentration in the bulk solution. If an equation like (21) were known a priori, then the total space-charge distribution in a pore could in principle be calculated from Equations (6) and (8) by knowing only pore radius and electrolyte concentration (that is, Debye length). A semilogarithmic plot of wall charge vs. potential is shown in Figure 8. Both charge and potential were determined from the conductivity data and the numerical calculations. The two membranes with larger pore sizes yield nearly identical wall charges for a given potential, although the relationship does not seem very linear. The 150 Å pore possesses a smaller charge, but the linearity of the data is quite good, and the slope ($\sim -z^*$) is approximately the same as for the larger pores. A quite tempting hypothesis to explain the differences between the small and large pores is that the chemical nature of the pore wall changes as the pore increases in size up to a point where curvature is unimportant. Such a hypothesis can be supported from the physics of pore formation in mica; etching curves obtained in our laboratory and that of others (Bean et al., 1970; Quinn et al., 1972) show that the pore growth rate (dr_o/dt) during the etching process does not become linear until r_o exceeds 100 to 200 Å, and Bean et al. specifically attribute the nonlinearity in growth to variations in the free energy of the solution/pore wall interface with pore radius.

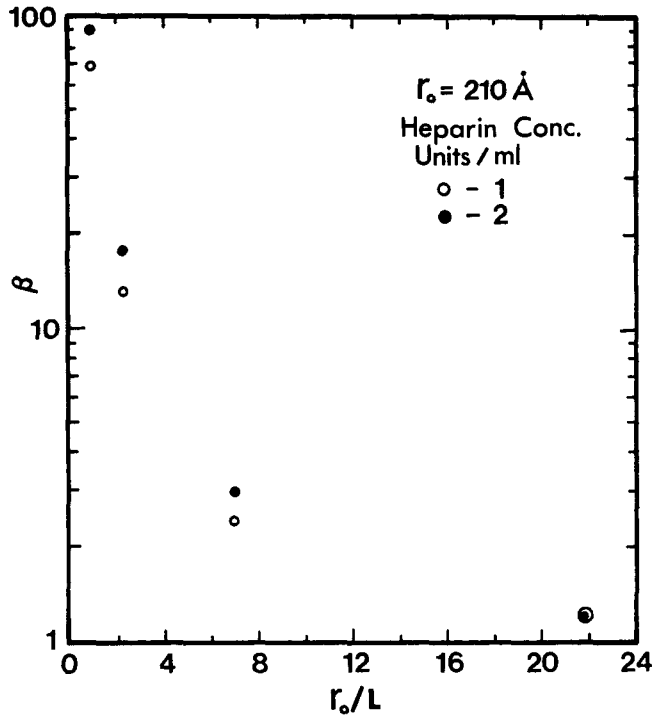

Fig. 9. Ratio of pore-to-bulk specific conductivity (β) vs. dimensionless pore radius for different heparin concentrations. The Debye length (L) was calculated from the measured bulk conductivity by assuming all electrolyte was potassium chloride.

If the heparin adsorption were not at a saturated state, then an increase in the wall charge would be expected if the bulk heparin concentration were increased. Enhanced conduction was measured for a membrane with pores 210 Å in radius for heparin concentrations of 1 and 2 units/cm^3 and potassium chloride concentrations of 10^{-4}-10^{-1} M. The data are shown in Figure 9 and clearly demonstrate that at the concentration levels used here the heparin adsorption was not at a saturated condition.

The real issue in our results is: Why do not the wall charges deduced from electroosmosis agree with those from enhanced conduction? For a given pore radius and electrolyte concentration, the same charge should have resulted for both, since the heparin concentration in the bulk solution was maintained constant throughout all runs, and presumably the double layer was in an equilibrium state. The important assumptions on which rest the validity of the classical double-layer electrokinetic model used here are: (1) direct ion-ion interactions are negligible (that is, ion activity coefficients equal unity); (2) solution properties such as dielectric constant and viscosity are constant and equal to their bulk values; (3) the charge at the pore wall (adsorbed heparin) is immobile and does not migrate under the influence of the applied electric field; and (4) the charge density at the pore wall is uniformly distributed.

Assumption (1) is necessary for application of the Boltzmann equation in a convenient form (Onsager, 1933). Essentially it says that each ion only interacts electrostatically with the field generated by the charged solid interface, and the effect of neighboring ions is indirect through space charge in the Poisson equation. A related assumption is that imaging, which accounts for the dielectric differences between solution and solid phase (mica in our case), provides only a small contribution to the free energy of an ion. [If the pore is uncharged, imaging may be important in very small pores, see, for example, Bean (1969).] Equation (4) is valid if the counterion density is small everywhere in the pore. To this end we restricted ourselves to dilute electrolyte solutions, but even at a bulk concentration of 10^{-2} M potassium chloride and a dimensionless potential equal to 4 the Boltzmann equation predicts a K^+ concentration of 0.27 M. At such moderate ion densities in the pore solution, self-atmosphere effects probably cause deviations of counterion activity coefficient from unity, but classical models which are usually based on Debye-Huckel theory cannot be used to correct the activity because they assume total solution electroneutrality. Although some error may be introduced in using the Boltzmann equation at these moderate concentrations, much of the error may actually cancel owing to opposing effects (Bolt, 1955; Levine and Bell, 1966).

The assumption of constant solvent viscosity and dielectric constant has received considerable attention in the literature (for example, Grahame, 1950; Conway et al., 1951; Lyklema and Overbeek, 1961). Solvent molecules are subject to polarization at large electric fields, thereby resulting in reduced molecular mobility. Such saturation effects are thought to be significant only at electric fields ($\partial\phi/\partial r$) above 1 000 statvolts/cm and probably influence double layer structure and electrokinetic phenomena only in the proximity of the charged interface. Since our computed charge densities were of the order 6 000 esu/cm^2, by Equation (8) the electric field perpendicular to the pore wall may have been large enough for such saturation effects to be appreciable near the wall itself, although the magnitude of the effect is difficult to predict.

A rather important but usually ignored aspect of double-layer theory is the distribution of fixed charge at the interface. If the adsorbed heparin were capable of migration, then the wall charge determined from the conduction measurements should be greater in magnitude than determined from electroosmosis; however, just the opposite observation was made (see Figure 7). Frumkin (1960) has raised doubts about the correctness of assuming a uniform charge density at the interface, and the problem has been treated quantitatively for a microscopically discrete but macroscopically uniform charge on a flat plate by Levine et al. (1972). It seems reasonable to expect that σ is discretely distributed, and the effect on electroosmosis may differ from that on conduction. For example, the adsorption of heparin may very well be localized at the more accessible regions of the pore wall (by assuming the pore is a rhombus) and absent in confined regions such as the obtuse corners where the electrostatic potential would be very high. Figure 6 illustrates the strong dependence of electroosmosis on pore geometry, so it is plausible to suspect that electroosmosis is quite dependent on wall-charge distribution.

On the basis of Figure 7 it is concluded that deficiencies exist in the classical electrokinetic model utilizing diffuse double-layer theory. Because the adsorption of heparin was not constant, our results do not provide as much information as originally desired. A significant improvement in the experiment should result if ion exchange groups could be covalently bonded to the mica pore wall; then the experimenter would be certain of a constant average σ as electrolyte concentration is varied.

ACKNOWLEDGMENT

This work was supported by NSF Grant GK-41279.

NOTATION

A_p = area of one pore, cm^2
B = shape parameter defined by Equation (A7)
$C_\pm$ = ion concentration, mole/cm^3

e = charge on electron, 4.8×10^{-10} esu
i_x = point axial current density, esu/cm²/s
I = current through the membrane, esu/s [=] 3.3×10^{-10} A
k = Boltzmann constant, 1.38×10^{-16} erg/molecule/°K
K = $\left[\frac{4\pi ze}{\epsilon kT}\right] r_o\sigma$
l = pore length
L = Debye length parameter [see Equation (7)], cm
n = number of pores in the membrane
N_o = Avogadro's number, 6.023×10^{23} mole^{-1}
P = pressure, dyne/cm²
Q = volumetric flow rate through the membrane, cm³/s
r = radial position in a circular pore, cm
r_o = pore radius (based on circle of equivalent area), cm
R = membrane resistance, (s/cm)$^{-1}$
T = temperature, °K
$\vec{U}$ = velocity field, cm/s
U_x = axial point velocity, cm/s
$V(x)$ = applied electric potential, statvolt [=] 300 V
w, y = Cartesian coordinates in a pore cross section, cm
x = axial coordinate in pore, cm
z = charge number of electrolyte

Greek Letters

α = electroosmotic flow coefficient [see Equation (15)], cm²/(s · statvolt)
β = enhanced conductivity ratio [see Equation (16)]
ϵ = solution dielectric constant
ζ = r/r_o for a circular pore
η = solution viscosity, g/(cm · s)
κ = solution specific conductance, s^{-1}
$<\kappa>$ = measured pore solution specific conductivity, s^{-1}
λ = κ_x/C_x, cm³/(mole · s)
(ξ, θ) = elliptical coordinates
ρ = solution density, g/cm³
ρ_e = solution space charge density, esu/cm³
σ = fixed charge density on the pore wall, esu/cm²
$\sigma(\alpha)$ = value of σ obtained by comparing electroosmotic flow data with numerical calculations, esu/cm²
$\sigma(\beta)$ = value of σ obtained by comparing enhanced conduction data with calculations, esu/cm²
ϕ = electrostatic part of Φ, statvolt [see Equation (3)]
Φ = total electrical potential, statvolt
Ψ = $ze\phi/kT$
Ψ_w = average value of Ψ at pore wall

Subscripts

∞ = bulk solution property
w = pore wall
x = axial direction in pore

LITERATURE CITED

Abendroth, R. P., "Surface Charge Development on Porous Silica in Aqueous Solution," *J. Phys. Chem.*, **76**, 2547 (1972).

Adamson, A. W., *Physical Chemistry*, 2 ed., Interscience, New York (1967).

Andrade, E. N. da C., and C. Dodd, "The Effect of an Electric Field on the Viscosity of Liquid," *Proc. Royal Soc.*, **A204**, 449 (1951).

Babchin, A. J., "Wedging Pressure in Solutions in Electrolytes Including the Effect of Electrostrictive Forces," *J. Colloid Interface Sci.*, **49**, 390 (1974).

Bean, C. P., "Characterization of Cellulose Acetate Membranes and Ultrathin Films for Reverse Osmosis," Office of Saline Water, Research and Development Report No. 465 (1969).

Bean, C. P., M. V., Doyle, and G. Entine, "Etching of Submicron Pores in Irradiated Mica," *J. Appl. Physics*, **41**, 1454 (1970).

Bolt, G. H., "Analysis of the Validity of the Gouy-Chapman Theory of the Electric Double Layer," *J. Colloid Sci.*, **10**, 206 (1955).

Booth, F., "The Dielectric Constant of Water and the Saturation Effect," *J. Chem. Phys.*, **19**, 391 (1951).

Buckingham, A. D., "Theory of the Dielectric Constant at High Field Strength," *Ibid.*, **25**, 428 (1956).

Conway, B. E., J. O'M. Bockris, and I. A. Ammar, "The Dielectric Constant of the Solution in the Diffuse and Helmholtz Double Layers at a Charged Surface in Aqueous Solution," *Trans. Faraday Soc.*, **47**, 756 (1951).

Davies, J. T., and E. K. Rideal, *Interfacial Phenomena*, Academic Press, New York (1961).

Dresner, L., "Electrokinetic Phenomena in Charged Microcapillaries," *J. Phys. Chem.*, **67**, 1635 (1963).

———, "The Exclusion of Ions from Charged Microporous Solids," *ibid.*, **69**, 2230 (1965).

Dukhin, S. S., and B. V. Derjaguin, "Equilibrium Double Layer and Electrokinetic Phenomena," in *Surface and Colloid Science*, E. Matijevic, ed., Vol. 7, p. 49, Wiley-Interscience, New York (1974).

Fair, J. C., and J. F. Osterle, "Reverse Electrodialysis in Charged Capillary Membranes," *J. Chem. Phys.*, **54**, 3307 (1971).

Finlayson, B. A., *The Method of Weighted Residuals and Variational Principles*, Chapt. 5, Academic Press, New York (1972).

Frumkin, A. N., "The Double Layer in Electrochemistry," *J. Electrochem. Soc.*, **107**, 461 (1960).

Grahame, D. C., "The Electrical Double Layer and the Theory of Electrocapillarity," *Chem. Rev.*, **41**, 441 (1947).

Grahame, D. C., "Effects of Dielectric Saturation Upon the Diffuse Double Layer and the Free Energy of Hydration of Ions," *J. Chem. Phys.*, **18**, 903 (1950).

Happel, J., and H. Brenner, *Low Reynolds Number Hydrodynamics*, pp. 495-497, Prentice-Hall, Englewood Cliffs, N. J. (1965).

Hoffer, E., and O. Kedem, "Ion Separation by Hyperfiltration through Charged Membranes. Calculation Based on TMS Model," *Ind. Eng. Chem. Process Design Develop.*, **11**, 221 (1972).

Helmholtz, H. L. F., *Ann. Physik*, **89**, 221 (1853).

Jacazio, G., R. F. Probstein, A. A. Sonin, and D. Young, "Electrokinetic Salt Rejection in Hyperfiltration through Porous Materials, Theory and Experiment," *J. Phys. Chem.*, **76**, 4015 (1972).

Levine, R. S., and G. M. Bell, "Modified Poisson-Boltzmann Equation and Free Energy of Electrical Double Layers in Hydrophobic Colloids," *Disc. Faraday Soc.*, No. 42, 69 (1966).

Levine, R. S., K. Robinson, G. M. Bell, and J. Mingins, "Discreteness-of-Charge Effect at Charged Aqueous Interfaces," *J. Electroanal. Chem. Interfacial Electrochem.*, **38**, 253 (1972).

Lyklema, J., and J. Th. G. Overbeek, "On the Interpretation of Electrokinetic Potentials," *J. Colloid Sci.*, **16**, 501 (1961).

Mackay, D., and P. Meares, "The Electrical Conductivity and Electroosmotic Permeability of a Cation-Exchange Resin," *Trans. Faraday Soc.*, **55**, 1221 (1959).

Melcher, J. R., and G. I. Taylor, "Electrohydrodynamics: A Review of the Role of Interfacial Shear Stresses," in *Annual Review of Fluid Mechanics*, W. R. Sears and M. van Dyke, ed., Vol. 1, p. 111 (1969) published by Annual Review Inc., Palo Alto.

Morrison, F. A., and J. F. Osterle, "Electrokinetic Energy Conversion in Ultrafine Capillaries," *J. Chem. Phys.*, **43**, 2111 (1965).

Newman, J. S., *Electrochemical Systems*, Prentice-Hall, Englewood Cliffs, N. J. (1973).

Onsager, L., "Theories of Concentrated Electrolytes," *Chem. Rev.*, **13**, 80 (1933).

Overbeek, J. Th. G., *Colloid Science*, H. R. Kruyt, ed., Vol. 1, Elsevier, Amsterdam (1952).

Quinn, J. A., J. L. Anderson, W. S. Ho, and W. J. Petzny, "Model Pores of Molecular Dimension—The Preparation and

Characterization of Track-etched Membranes," *Biophys. J.*, **12**, 990 (1972).
Reeves, R. M., "The Electrical Double Layer: The Current Status of Data and Models, with Particular Emphasis on the Solvent," in *Modern Aspects of Electrochemistry*, B. E. Conway and J. O'M. Bockris, ed., Vol. 9, p. 239, Plenum, New York (1974).
Rutgers, A. J., and M. de Smet, "Electroosmosis, Streaming Potentials, and Surface Conductance," *Trans. Faraday Soc.*, **43**, 102 (1947).
Sparnaay, M. J., "Ion-size Corrections of the Poisson-Boltzmann Equation," *Electroanal. Chem. Interfacial Electrochem.*, **37**, 65 (1972).
Stern, O., "Zur Theorie der Electrolytischen Doppelschicht," *Z. Elektrochem.*, **30**, 508 (1924).
Stoner, G. E., S. Srinivasan, and E. Gileadi, "Adsorption Inhibition as a Mechanism for the Antithrombogenic Activity of Some Drug-Competitive Adsorption of Fibrinogen and Heparin on Mica," *J. Phys. Chem.*, **75**, 2107 (1971).
Verwey, E. J. W., and J. Th. G. Overbeek, *Theory of the Stability of Lyophobic Colloids*, Elsevier, Amsterdam (1948).
Weast, R. C., ed., *Handbook of Chemistry and Physics*, 51 ed., Chemical Rubber Co., Cleveland (1971).

APPENDIX

Circular, Cylindrical Pore

Because of angular uniformity, the equations for electrostatic potential and axial electroosmotic velocity are ordinary differential equations. Equation (6) and boundary condition (8) become

$$\frac{1}{\zeta}\frac{d}{d\zeta}\left(\zeta\frac{d\Psi}{d\zeta}\right) = \left(\frac{r_o}{L}\right)^2 \sinh(\Psi)$$

$$\zeta = 1: \quad \frac{d\Psi}{d\zeta} = \left(\frac{4\pi z e}{\epsilon kT}\right) r_o\sigma \equiv K \tag{A1}$$

$$\zeta = 0: \quad \frac{d\Psi}{d\zeta} = 0$$

where ζ is the dimensionless radial position (r/r_o). The momentum Equation (11) reduces to

$$\frac{1}{\zeta}\frac{d}{d\zeta}\left(\zeta\frac{dU_x}{d\zeta}\right) = \frac{1}{\eta}\left(\frac{\epsilon kT}{4\pi z e}\right)\left(\frac{r_o}{L}\right)^2 \sinh(\Psi)\,[-V'(x)]$$

$$\zeta = 1: \quad U_x = 0 \tag{A2}$$

$$\zeta = 0: \quad \frac{dU_x}{d\zeta} = 0$$

Equation (7) has been used to eliminate C_x, and an applied electric field $[-V'(x)]$ of 1 statvolt/cm is assumed as the basis for the linear driving force. In all calculations the solvent is water, and the following constants are assigned: $\epsilon = 78$, $z = 1$, $T = 298°$K, $\eta = 0.0089$ poise. In Equations (A1) and (A2) the variable parameters of interest are K and r_o/L.

Equation (A1) was solved by a fourth-order Runge-Kutta shooting scheme. The velocity profile was then calculated by direct integration [eliminate $(r_o/L)^2 \sinh(\Psi)$ in (A2) by using (A1)]. Pore area integrations were performed by using Simpson's formula.

An analytical solution to (A1) is possible if $\sinh(\Psi)$ is replaced by $\exp(\Psi)/2$:

$$\Psi(\zeta) = \ln\left[\frac{16K}{(4+K)(r_o/L)^2}\right] - 2\ln\left[1 - \frac{K\zeta^2}{4+K}\right] \tag{A3}$$

This solution is valid when $\Psi > 1$ for all ζ, or more precisely when

$$\frac{r_o}{L} < 2.5\left[\frac{K}{4+K}\right]^{1/2} \tag{A4}$$

The electrokinetic parameters α and β are easily computed by using Equation (A3), and this solution was used for pores meeting criterion (A4) to eliminate unnecessary machine computation:

$$\alpha = \left(\frac{\epsilon kT}{2\pi\eta z e}\right)\left[\frac{4+K}{K}\ln\left(\frac{4+K}{4}\right) - 1\right] \tag{A5}$$

$$\beta = \frac{2K}{(r_o/L)^2}\left\{1 + \frac{\epsilon RT}{\pi\eta\lambda}\left[\frac{4}{K}\ln\left(\frac{4}{4+K}\right) + 1\right]\right\} \tag{A6}$$

Elliptical, Cylindrical Pore

Elliptical coordinates (Happel and Brenner, 1965) are orthogonal and properly define the pore wall. The Poisson-Boltzmann equation becomes

$$\frac{\partial^2\Psi}{\partial\xi^2} + \frac{\partial^2\Psi}{\partial\theta^2} = \left(\frac{r_o}{L}\right)^2 B^2\,[\sinh^2(\xi) + \sin^2(\theta)]\sinh(\Psi)$$

$$\theta = 0, \pi/2: \quad \frac{\partial\Psi}{\partial\theta} = 0$$

$$\xi = 0: \quad \frac{\partial\Psi}{\partial\xi} = 0 \tag{A7}$$

$$\xi = \xi_o \text{ (pore wall)}: \quad \frac{\partial\Psi}{\partial\xi} = B\,[\sinh^2(\xi_o) + \sin^2(\theta)]^{1/2} K$$

$$B \equiv [\cosh^2(\xi_o)\tanh(\xi_o)]^{-1/2}$$

θ is analogous to a cylindrical angle, while $\xi =$ constant is an ellipse of eccentricity $[\tanh(\xi)]^{-1}$. The parameter K has the same value as it does for a circular pore, where r_o is the radius of a circle of area equivalent to the ellipse. The pore shape is determined by ξ_o which was chosen as 0.4147 here so that the ellipse would have the same perimeter-to-area ratio as a 60 deg. rhombus. The parameters are K and r_o/L as for the circle. Equation (A7) was solved by using a mixed collocation/Runge-Kutta scheme (Finlayson, 1972). The potential was approximated by an even polynomial in θ of degree 8, with the coefficients being a function of ξ. The polynomial approximation was forced to satisfy both boundary conditions on θ for any ξ. The four necessary collocation values of θ were evenly distributed ($\pi/16$, $3\pi/16$, $5\pi/16$, $7\pi/16$); values for Ψ at these θ values as a function of ξ were obtained by using a shooting, fourth-order Runge-Kutta scheme. Numerical convergence was assured by comparing the potential profile from the four-point collocation for $r_o/L = 1$, with a three-point collocation approximation; negligibly small differences were found.

Again, for the axial velocity a basis of $-V'(x) = 1$ statvolt/cm driving force was used to obtain the numerical solution

$$\frac{\partial^2 U_x}{\partial\xi^2} + \frac{\partial^2 U_x}{\partial\theta^2} = \frac{B^2}{\eta}\left(\frac{r_o}{L}\right)^2\left(\frac{\epsilon kT}{4\pi z e}\right)$$
$$[\sinh^2(\xi) + \sin^2(\theta)]\sinh(\Psi)\,[-V'(x)]$$

$$\theta = 0, \pi/2: \quad \frac{\partial U_x}{\partial\theta} = 0 \tag{A8}$$

$$\xi = 0: \quad \frac{\partial U_x}{\partial\xi} = 0$$

$$\xi = \xi_o \text{ (pore wall)}: \quad U_x = 0$$

Because $\Psi(\xi, \theta)$ was known from the solution to (A7), the above equation was easily solved by using a straightforward finite difference method with a Newton-Raphson correction for the guessed grid line $\xi = 0$. [With linear equations such as (A8), the correction converges the first time to the proper value of the grid line potentials.] A check on the finite difference scheme was made by substituting $\Psi =$ constant into (A8), since the analytical solution for U_x and $\langle U_x\rangle$ are known for this case; the calculations agreed within 0.5% of the analytical solution. Pore area integrations were performed by using the two-variable Simpson's formula.

Manuscript received April 29, 1975; revision received July 15, and accepted July 25, 1975.